actuators

MDPI

Article

Adaptive Multi-Parameter Estimation of Inertial Stabilization Platform with Unknown Load

Jieji Zheng, Xin Xie *, Baoyu Li, Ziping Wan, Ning Chen and Dapeng Fan

College of Intelligence Science and Technology, National University of Defense Technology, Changsha 410073, China
* Correspondence: xiexin12@nudt.edu.cn; Tel.: +86-137-8704-3604

Abstract: In order to improve the state monitoring and adaptive control capability of inertial stabilization platforms (ISPs) with unknown loads, it is necessary to estimate the dynamic parameters comprehensively online. However, most current online estimation methods regard the system as a linear dual-inertia model which neglects the backlash and nonlinear friction torque. It reduces the accuracy of the model and leads to incomplete and low accuracy of the estimated parameters. The purpose of this research is to achieve a comprehensive and accurate online estimation of multiple parameters of ISPs and lay a foundation for state monitoring and adaptive control of ISPs. First, a dual-inertia model containing backlash and nonlinear friction torque of the motor and load is established. Then, the auto-regressive moving average (ARMA) model of the motor and load is established by the forward Euler method, which clearly expresses the online identification formula of the parameters. On this basis, the adaptive identification method based on the recursive extended least squares (RELS) algorithm is used to realize the online estimation of multiple parameters. The simulation and experimental results show that the proposed adaptive multi-parameter estimation method can realize the simultaneous online identification of the moment of inertia of the load, the damping coefficient of motor and load, the transmission stiffness, the Coulomb friction torque of motor and load, and the backlash, and the steady-state error is less than 10%. Compared with the traditional linear dual-inertia model, the similarity between the model based on the proposed adaptive parameter estimation algorithm and the actual system is increased by 65.3%.

Keywords: inertial stabilization platform; backlash; nonlinear friction torque; adaptive multi-parameter estimation

Citation: Zheng, J.; Xie, X.; Li, B.; Wan, Z.; Chen, N.; Fan, D. Adaptive Multi-Parameter Estimation of Inertial Stabilization Platform with Unknown Load. *Actuators* **2023**, *12*, 176. https://doi.org/10.3390/act12040176

Academic Editor: Liang Sun

Received: 11 March 2023
Revised: 10 April 2023
Accepted: 13 April 2023
Published: 18 April 2023

1. Introduction

Inertial stabilization platforms (ISPs) play an increasingly important role in the field of remote sensing, such as optical imaging equipment, tracking radar, antenna, and so on [1–6], to isolate the influence of carrier motion on pointing accuracy. With the increase in load weight range (10 kg~100 kg), ISPs need a precision reducer to enlarge the driving torque and ensure high transmission accuracy. However, the reducer would inevitably introduce backlash and nonlinear friction torque [7–9]. At the same time, ISPs would collocate different loads according to different tasks, resulting in changes in the resonance frequency, stability margin, and nonlinear characteristics of the system, and ultimately deteriorating the security and control performance of ISPs [10,11].

To solve this problem, there are two main solutions used in engineering now. One is to design a controller with sufficient margin to ensure robustness when the load changes, while sacrificing the dynamic performance of the system. The other is to redesign all parameters of the servo control system after each load modification, which has the disadvantages of low efficiency and high cost. To make up for the shortcomings of the above two ways, researchers gradually turned their attention to adaptive control, which can automatically adjust the structure or parameters of the controller according to the information collected by the sensors, to maintain the performance of the system [10,12–14]. Nevertheless, the basis of adaptive control is to estimate the key dynamic parameters of the system online according to the information collected by sensors. Thus, a lot of research has been carried out on adaptive parameter estimation.

Ref. [15] presented a moment of inertia (MOI) identification method based on the improved model-reference adaptive system that uses a dynamic gain and a curvature model, which not only decreases the identification error caused by the load torque but also ensures fast convergence speed and high identification accuracy. Liu [16] compared the effects of various parameters on the running stability of the motor, and a least-squares identification method based on the forgetting factor is added to identify the parameter online to optimize the prediction model in real time. Kim [17] proposed a new method of servo system parameter identification, in which the MOI, Coulomb friction torque, and viscous coefficient of the servo device can be obtained from the half-cycle integration of the extremely low-frequency sinusoidal torque command. To solve the problem that the mismatch of the parameters of the permanent magnet synchronous motor (PMSM) drive system would lead to the observation error of the load torque, Lian C [18] proposed two identification methods: the direct calculation method and the proportional-integral (PI) regulator method, so that the load torque observer also has a higher observation accuracy and faster convergence speed. Yang M [19] proposed an adaptive Kalman Observer Recursive Least Square identification method based on the original Kalman Observer and recursive least squares (RLS) by adding an adaptive algorithm, which can achieve better performance and improve robustness under time-varying load and inaccurate initial value conditions. For the problem of online frequency domain identification of mechanical systems with variable dynamic characteristics, Nevaranta [20] proposed a closed-loop frequency domain online identification algorithm based on sliding discrete Fourier transform on selected frequency groups and the simulation and test results show that the algorithm can obtain satisfactory real-time frequency response estimation in short data using sliding windows. Amini [21] presented the simultaneous integration of online estimation of structural parameters with adaptive control to reduce structural vibrations, in which the stiffness and damping online identification were carried out by the RLS method without initial estimation and only by measuring the structural responses. To solve the problem of simultaneous state estimation and parameter identification for a class of nonlinear systems, Alvaro-Mendoza [22] designed an adaptive observer based on the sliding mode method, whose main advantages are that it combines the robustness and finite-time convergence of the sliding mode observer, as well as the simple tuning of the high-gain observer, reducing the tuning effort. In addition, some researchers have adopted intelligent algorithms, such as particle swarm optimization (PSO), genetic algorithm (GA), neural network algorithm (NNA), and other intelligent algorithms to realize online parameter identification and have made some breakthroughs [23–25].

Summarizing the various identification methods proposed above, the following deficiencies can be found:

(1) In order to reduce the parameters to be identified, many studies simplified the dynamic model to a first-order model, which reduces the accuracy of the model and leads to the low accuracy of parameter identification.
(2) For the dual-inertia dynamic model with backlash and a nonlinear friction torque of motor and load, the explicit expression for online identification of parameters has not been seen.

Therefore, the above methods cannot distinguish the varieties of system characteristics when the load changes, thus reducing the accuracy of identification. In order to make up for the above two deficiencies, the following works were carried out in this study:

(1) An adaptive estimation method of the dual-inertia model considering the backlash and nonlinear friction torque of motor and load is proposed.
(2) The explicit solutions of all model parameters in the online estimation process are obtained.

(3) The multi-parameter online identification method proposed in this manuscript can achieve simultaneous online identification of nine key dynamic parameters, including load MOI, transmission stiffness, motor viscous damping coefficient, load viscous damping coefficient, Coulomb friction torque of motor forward and reverse, Coulomb friction torque of load forward and reverse, and transmission backlash.

This research can finally realize the simultaneous online identification of load MOI, motor damping coefficient, load damping coefficient, transmission stiffness, Coulomb friction torque of motor and load, and backlash, which greatly improved the fitting degree between the proposed model and the actual system. The other parts of this paper are as follows: In Section 2, the nonlinear dynamic model framework of the ISP is constructed, and the adaptive multi-parameter estimation method is proposed in Section 3. Section 4 carries out simulation and experimental verification of the effectiveness of the adaptive multi-parameter estimation method. Section 5 gives the summary of this paper.

2. Problem Statement

Figure 1 shows the structure of the two-axis inertial stabilization platform, and the elevation gimbal is installed inside the azimuth gimbal. The azimuth gimbal controls the azimuth motion of the line of sight (LOS) through a motor-driving gear ring, while the elevation gimbal controls the elevation motion of the LOS through a precision reducer. When the load modifies, the direct impact is the change in the moment of inertia at the output side of the reducer. Since the weight of the azimuth gimbal is far greater than the total weight of the elevation gimbal and the load, the change in load has little effect on the azimuth gimbal. Therefore, we take the elevation gimbal as the object of this paper.

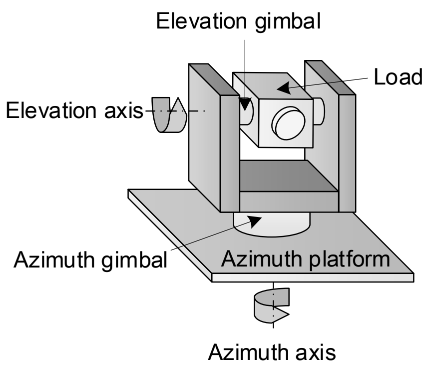

Figure 1. The structure of the two-axis inertial stabilization platform.

The elevation gimbal consists of a driver, a motor, a reducer, a load, and an encoder, as shown in Figure 2, and the load can be flexibly replaced. In the figure, u is the voltage command input to the actual system and model, K_{I} is the conversion coefficient of the driver, K_{T} is the motor torque factor, and J_m, J_L are the moment of inertia of the motor and load, respectively; N is the transmission ratio of the reducer, K_s is the transmission stiffness, and θ_m, ω_m are the angular and angular velocity of the motor, respectively; θ_L, ω_L are the angular and angular velocity of the load, respectively; T_{fm}, T_{fL} are the nonlinear friction torque of the motor and load, respectively; T_q is the transmission torque of the reducer.

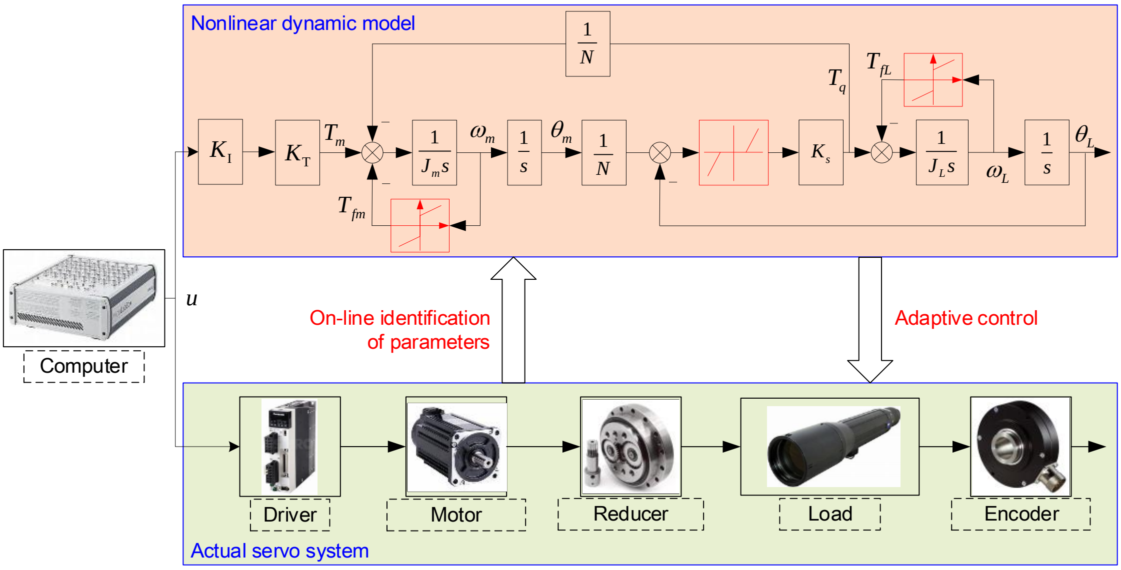

Figure 2. Nonlinear dynamic model framework.

According to Figure 2, the dynamic model of the system can be expressed as:

$$\begin{cases} \dot{\theta}_m = \omega_m \\ J_m \dot{\omega}_m = u K_{\mathrm{I}} K_{\mathrm{T}} - \frac{1}{N} T_q - T_{fm} \\ \dot{\theta}_L = \omega_L \\ J_L \dot{\omega}_L = T_q - T_{fL} \end{cases}. \tag{1}$$

To facilitate the analysis, previous studies simplified the friction of the motor and load into the linear viscous friction. However, this simplification makes it unable to describe the details of the actual system at low speed or when the direction is reversed. In this paper, the friction of the motor and load are both expressed in the form of Coulomb friction plus viscous friction, as shown in Equation (2).

$$T_{fm} = \begin{cases} T_{cm}^{+} + B_m \omega_m & \omega_m > 0 \\ 0 & \omega_m = 0 \\ T_{cm}^{-} + B_m \omega_m & \omega_m < 0 \end{cases}, \; T_{fL} = \begin{cases} T_{cL}^{+} + B_L \omega_L & \omega_L > 0 \\ 0 & \omega_L = 0 \\ T_{cL}^{-} + B_L \omega_L & \omega_L < 0 \end{cases}, \tag{2}$$

where T_{cm}^{+}, T_{cm}^{-} are the Coulomb friction of the motor in different directions; T_{cL}^{+}, T_{cL}^{-} are the Coulomb friction of the load in different directions; and B_m, B_L are the viscous coefficient of the motor and load, respectively. Since there is backlash in the reducer, the dead zone model is adopted to describe the transmission torque, as shown in Equation (3).

$$T_q = \begin{cases} K_s(z - \Delta) & z > \Delta \\ 0 & |z| < \Delta \\ K_s(z + \Delta) & z < -\Delta \end{cases}, \; z = \frac{\theta_m}{N} - \theta_L, \tag{3}$$

where z is the transmission error and Δ is the backlash of the reducer.

By considering the dead zone and the nonlinear friction torque, the fitting degree between the dynamic model and the actual system can be greatly improved, and the detailed characteristics of the system at low speed can be better depicted. According to Figure 2, to achieve live updating of the dynamic model, a total of nine parameters need to be identified online, which include J_L, B_m, B_L, K_s, T_{cm}^{+}, T_{cm}^{-}, T_{cL}^{+}, T_{cL}^{-}, and Δ. However, as far as the authors know, there is no algorithm that can realize online recognition of so many parameters at the same time. Hence, the aim of this paper is to realize the simultaneous online identification of the above nine parameters, which lays the foundation for the state monitoring and adaptive control of the ISPs.

3. Multi-Parameter Online Identification Method

According to Equation (2), the Coulomb friction in different directions can be shown as:

$$T_c = \begin{cases} T_c^+ & \omega > 0 \\ 0 & \omega = 0, \\ T_c^- & \omega < 0 \end{cases} \tag{4}$$

where ω is the velocity. To identify the Coulomb friction of the motor and load, it is necessary to linearize it. Then, we define the following functions:

$$\begin{cases} \widetilde{\omega}^+ = \frac{1}{2}\mathrm{sign}(\omega)(1+\mathrm{sign}(\omega)) \\ \widetilde{\omega}^- = -\frac{1}{2}\mathrm{sign}(\omega)(1-\mathrm{sign}(\omega)) \end{cases}, \tag{5}$$

where $\widetilde{\omega}^+$ and $\widetilde{\omega}^-$ are the equivalent velocities. According to Equations (2), (4), and (5), the Coulomb friction of motor and load can be expressed as:

$$\begin{cases} T_{cm} = T_{cm}^+\widetilde{\omega}_m^+ + T_{cm}^-\widetilde{\omega}_m^-, \\ T_{cL} = T_{cL}^+\widetilde{\omega}_L^+ + T_{cL}^-\widetilde{\omega}_L^- \end{cases} \tag{6}$$

where the right subscripts m and L of $\widetilde{\omega}$ represent the equivalent speed of motor and load, respectively. By introducing Equations (3) and (6) into Equation (1) and temporarily ignoring the backlash of the system, the dynamic Equations can be obtained as:

$$\begin{aligned} &\dot{\theta}_m = \omega_m \\ &J_m\dot{\omega}_m = uK_\mathrm{I}K_\mathrm{T} - \frac{1}{N}K_s\left(\frac{1}{N}\theta_m - \theta_L\right) - B_m\omega_m - T_{cm}^+\widetilde{\omega}_m^+ - T_{cm}^-\widetilde{\omega}_m^- \\ &\dot{\theta}_L = \omega_L \\ &J_L\dot{\omega}_L = K_s\left(\frac{1}{N}\theta_m - \theta_L\right) - B_L\omega_L - T_{cL}^+\widetilde{\omega}_L^+ - T_{cL}^-\widetilde{\omega}_L^- \end{aligned} . \tag{7}$$

Establishing the state vector as $x = [\theta_m, \omega_m, \theta_L, \omega_L]^\mathrm{T}$, Equation (7) can be converted into a continuous state space as:

$$\dot{x} = Ax + Bu + C\begin{bmatrix} T_{cm}^+\widetilde{\omega}_m^+ + T_{cm}^-\widetilde{\omega}_m^- \\ T_{cL}^+\widetilde{\omega}_L^+ + T_{cL}^-\widetilde{\omega}_L^- \end{bmatrix}, \tag{8}$$

where,

$$A = \begin{bmatrix} 0 & 1 & 0 & 0 \\ -\frac{K_s}{N^2J_m} & -\frac{B_m}{J_m} & \frac{K_s}{NJ_m} & 0 \\ 0 & 0 & 0 & 1 \\ \frac{K_s}{NJ_L} & 0 & -\frac{K_s}{J_L} & -\frac{B_L}{J_L} \end{bmatrix}, B = \begin{bmatrix} 0 \\ \frac{K_\mathrm{I}K_\mathrm{T}}{J_m} \\ 0 \\ 0 \end{bmatrix}, C = \begin{bmatrix} 0 & 0 \\ -\frac{1}{J_m} & 0 \\ 0 & 0 \\ 0 & -\frac{1}{J_L} \end{bmatrix}.$$

To realize online identification in practical digital systems, it is necessary to discretize the continuous state space. Since the expression of the fourth-order matrix discretized by the zero-order holder is too complex, it would cause a great computational burden to the computer and cannot obtain the expression of the online identification of parameters. In this paper, the forward Euler method is proposed to discretize the continuous state space and the discretization process is as follows:

$$\begin{cases} A_d = \mathbf{I}_{4\times4} + AT_s \\ B_d = BT_s \\ C_d = CT_s \end{cases}, \tag{9}$$

where $\mathbf{I}_{4\times4}$ is the identity matrix and T_s is the discrete sampling period. The state space of the discrete domain can be obtained as follows:

$$x(k+1) = A_d x(k) + B_d u(k) + C_d \begin{bmatrix} T_{cm}^{+}\widetilde{\omega}_m^{+}(k) + T_{cm}^{-}\widetilde{\omega}_m^{-}(k) \\ T_{cL}^{+}\widetilde{\omega}_L^{+}(k) + T_{cL}^{-}\widetilde{\omega}_L^{-}(k) \end{bmatrix}, \tag{10}$$

where k is the sample counter, and

$$A_d = \begin{bmatrix} 1 & T_s & 0 & 0 \\ -\frac{K_s T_s}{N^2 J_m} & -\frac{B_m T_s}{J_m}+1 & \frac{K_s T_s}{N J_m} & 0 \\ 0 & 0 & 1 & T_s \\ \frac{K_s T_s}{N J_L} & 0 & -\frac{K_s T_s}{J_L} & -\frac{B_L T_s}{J_L}+1 \end{bmatrix}, B_d = \begin{bmatrix} 0 \\ \frac{K_I K_T T_s}{J_m} \\ 0 \\ 0 \end{bmatrix}, C_d = \begin{bmatrix} 0 & 0 \\ -\frac{T_s}{J_m} & 0 \\ 0 & 0 \\ 0 & -\frac{T_s}{J_L} \end{bmatrix}.$$

Then, the ARMA models of the motor and load are obtained as shown in Equations (11) and (12), respectively.

$$\begin{aligned} \omega_m(k+1) = {} & \frac{J_m - B_m T_s}{J_m}\omega_m(k) - \frac{K_s T_s}{N^2 J_m}\theta_m(k) + \frac{K_s T_s}{N J_m}\theta_L(k) \\ & + \frac{K_I K_T T_s}{J_m}u(k) - \frac{T_s}{J_m}(T_{cm}^{+}\widetilde{\omega}_m^{+}(k) + T_{cm}^{-}\widetilde{\omega}_m^{-}(k)) \end{aligned}, \tag{11}$$

$$\begin{aligned} \omega_L(k+1) = {} & \frac{J_L - B_L T_s}{J_L}\omega_L(k) + \frac{K_s T_s}{N J_L}\theta_m(k) - \frac{K_s T_s}{J_L}\theta_L(k) \\ & - \frac{T_s}{J_L}(T_{cL}^{+}\widetilde{\omega}_L^{+}(k) + T_{cL}^{-}\widetilde{\omega}_L^{-}(k)) \end{aligned}. \tag{12}$$

In this paper, a recursive extended least squares (RELS) algorithm is adopted to realize the iterative update of ARMA model parameters. With the voltage, the angular and angular velocity of the motor as the input, the recursive state vector of the motor is constructed as shown in Equation (13):

$$\begin{aligned} \mathbf{\Phi}_1 &= \left[-\omega_m(k), \theta_m(k), \theta_L(k), u(k), \widetilde{\omega}_m^{+}(k), \widetilde{\omega}_m^{-}(k)\right]^{\mathrm{T}}, \\ \mathbf{\Theta}_1 &= \left[\frac{B_m T_s - J_m}{J_m}, -\frac{K_s T_s}{N^2 J_m}, \frac{K_s T_s}{N J_m}, \frac{K_I K_T T_s}{J_m}, -\frac{T_{cm}^{+} T_s}{J_m}, -\frac{T_{cm}^{-} T_s}{J_m}\right]^{\mathrm{T}} \end{aligned}, \tag{13}$$

where $\mathbf{\Phi}_1$, $\mathbf{\Theta}_1$ are the state vector and regression vector, respectively. Thus, Equation (11) is converted into:

$$\omega_m(k+1) = \mathbf{\Phi}_1^{\mathrm{T}}\mathbf{\Theta}_1. \tag{14}$$

Then, the iterative process of RELS for obtaining motor parameters is shown as follows [26]:

$$\begin{cases} \hat{\mathbf{\Theta}}_1(k+1) = \hat{\mathbf{\Theta}}_1(k) + \mathbf{K}_1(k+1)\left[\omega_m(k+1) - \mathbf{\Phi}_1^{\mathrm{T}}(k+1)\hat{\mathbf{\Theta}}_1(k)\right] \\ \mathbf{K}_1(k+1) = \frac{\mathbf{P}_1(k)\mathbf{\Phi}_1(k+1)}{\lambda + \mathbf{\Phi}_1^{\mathrm{T}}(k+1)\mathbf{P}_1(k)\mathbf{\Phi}_1(k+1)} \\ \mathbf{P}_1(k+1) = \frac{1}{\lambda}\left[\mathbf{I} - \mathbf{K}_1(k+1)\mathbf{\Phi}_1^{\mathrm{T}}(k+1)\right]\mathbf{P}_1(k) \end{cases}, \tag{15}$$

where $\mathbf{K}_1(k+1)$ is the recursive gain, $\mathbf{P}_1(k+1)$ is the covariance matrix of estimation deviation, and λ is the forgetting factor.

Similarly, the state vector $\mathbf{\Phi}_2$ and regression vector $\mathbf{\Theta}_2$ of the load can be constructed as shown in Equation (14):

$$\begin{aligned} \mathbf{\Phi}_2 &= \left[-\omega_L(k), \theta_m(k), \theta_L(k), \widetilde{\omega}_L^{+}(k), \widetilde{\omega}_L^{-}(k)\right]^{\mathrm{T}}, \\ \mathbf{\Theta}_2 &= \left[\frac{B_L T_s - J_L}{J_L}, \frac{K T_s}{N J_L}, -\frac{K T_s}{J_L}, -\frac{T_c^{+} T_s}{J_L}, -\frac{T_c^{-} T_s}{J_L}\right]^{\mathrm{T}} \end{aligned}. \tag{16}$$

And Equation (12) is converted into:

$$\omega_L(k+1) = \mathbf{\Phi}_2^{\mathrm{T}}\mathbf{\Theta}_2. \tag{17}$$

Then, the iterative process for obtaining load parameters is shown as follows [26]:

$$\left\{\begin{array}{l}\hat{\mathbf{\Theta}}_2(k+1)=\hat{\mathbf{\Theta}}_2(k)+\mathbf{K}_2(k+1)\left[\omega_L(k+1)-\mathbf{\Phi}_2^{\mathrm{T}}(k+1)\hat{\mathbf{\Theta}}_2(k)\right] \\ \mathbf{K}_2(k+1)=\frac{\mathbf{P}_2(k)\mathbf{\Phi}_2(k+1)}{\lambda+\mathbf{\Phi}_2^{\mathrm{T}}(k+1)\mathbf{P}_2(k)\mathbf{\Phi}_2(k+1)} \\ \mathbf{P}_2(k+1)=\frac{1}{\lambda}\left[\mathbf{I}-\mathbf{K}_2(k+1)\mathbf{\Phi}_2^{\mathrm{T}}(k+1)\right]\mathbf{P}_2(k)\end{array}\right. \tag{18}$$

By combining Equations (13) and (16), we can get the estimation Equations of the following eight parameters:

$$\begin{array}{l}\hat{J}_L=-\frac{NJ_m\hat{\mathbf{\Theta}}_1(3)}{\hat{\mathbf{\Theta}}_2(3)},\hat{B}_m=\frac{J_m\left(\hat{\mathbf{\Theta}}_1(1)+1\right)}{T_s},\hat{B}_L=-\frac{NJ_m\hat{\mathbf{\Theta}}_1(3)\left(\hat{\mathbf{\Theta}}_2(1)+1\right)}{T_s\hat{\mathbf{\Theta}}_2(3)},\hat{K}_s=\frac{NJ_m\hat{\mathbf{\Theta}}_1(3)}{T_s} \\ \hat{T}_{cm}^{+}=-\frac{J_m\hat{\mathbf{\Theta}}_1(5)}{T_s},\hat{T}_{cm}^{-}=-\frac{J_m\hat{\mathbf{\Theta}}_1(6)}{T_s},\hat{T}_{cL}^{+}=\frac{NJ_m\hat{\mathbf{\Theta}}_1(3)\hat{\mathbf{\Theta}}_2(4)}{T_s\hat{\mathbf{\Theta}}_2(3)},\hat{T}_{cL}^{-}=\frac{NJ_m\hat{\mathbf{\Theta}}_1(3)\hat{\mathbf{\Theta}}_2(5)}{T_s\hat{\mathbf{\Theta}}_2(3)}\end{array}, \tag{19}$$

where $\hat{J}_L$, $\hat{B}_m$, $\hat{B}_L$, $\hat{K}_s$, $\hat{T}_{cm}^{+}$, $\hat{T}_{cm}^{-}$, $\hat{T}_{cL}^{+}$, and $\hat{T}_{cL}^{-}$ are the estimated values of J_L, B_m, B_L, K_s, T_{cm}^{+}, T_{cm}^{-}, T_{cL}^{+}, and T_{cL}^{-}, respectively. The moment of inertia in the motor can be obtained from the product description. Thus, it can be considered as a known parameter.

In addition, in order to estimate the backlash in real time, we proposed an online backlash test method, as shown in Figure 3. In Figure 3, ω_m' and ω_L' are the test values of ω_m and ω_L in the actual system, respectively. The principle is to capture the time t_1 when the drive component and driven component are disconnected and the time t_2 when they are reconnected and calculate the size of the backlash accordingly.

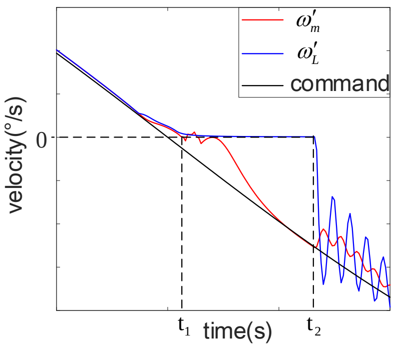

Figure 3. Principle of the online backlash test method.

According to Figure 3, we put forward a method to accurately capture t_1 and t_2, which are shown in Equations (20) and (21), respectively.

$$\begin{array}{ll}\text{if} & |\omega_m'(t-n_1)|>\omega_0\&|\omega_m'(t-n_1+1)|<\omega_0\&\cdots\&|\omega_m'(t)|<\omega_0 \\ & t_1=t-n_1+1 \\ \text{end} & \end{array}, \tag{20}$$

$$\begin{array}{ll}\text{if} & |\omega_L'(t-n_1)|<\omega_0\&|\omega_L'(t-n_1+1)|<\omega_0\&\cdots\&|\omega_L'(t)|>\omega_0 \\ & t_2=t \\ \text{end} & \end{array}, \tag{21}$$

where t is the current moment, n_1 is set to ensure the reliability of the method, and ω_0 is the speed threshold to judge whether the motor and load reverse. When the velocity is less than ω_0, the motor or the load is considered to be reversed. Then, the size Δ of backlash can be calculated by Equation (22).

$$2\Delta=\left|\theta_m'(t_1)-\theta_m'(t_2)\right|+\left|\theta_L'(t_1)-\theta_L'(t_2)\right|, \tag{22}$$

where θ_m', θ_L' are the angular of the motor and load collected by encoders, respectively.

The advantage of this method is that the backlash can be calculated only once the velocity reverses, which is practical for the equipment with a frequent reversal.

4. Simulation and Experimental Verification

To verify the effectiveness of the multi-parameter online identification method, an experimental platform was built, and a series of simulations and tests were carried out. As shown in Figure 4, the experimental platform is mainly composed of a permanent magnet synchronous motor (model: ASM80B1007-30M), an RV reducer (model: ZKRV-20E-161-B), a moment of inertia adjusting device, and an absolute encoder (model: BCE112K50). The adjusting device is used to simulate the load of the ISP. The following values of the actual system are obtained by consulting the instructions of the experimental equipment and 3D modeling: $K_I = 0.48$ A·V^{-1}, $K_T = 0.49$ Nm·A^{-1}, $N = 161$, and $J_m = 2 \times 10^{-4}$ kg·m^2. When there is no mass block, the no-load condition of the ISP is simulated, and there is $J_L = 0.22$ kg·m^2. After adding the mass blocks, the simulated case is with load, and the moment of inertia becomes $J_L = 0.45$ kg·m^2.

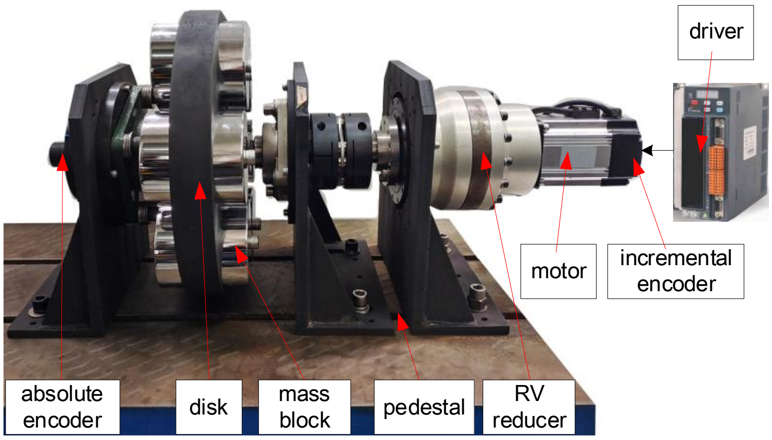

Figure 4. The experimental platform.

4.1. Simulation Analysis

According to the dynamic model established in Section 2, the simulation model was built in Simulink. In addition to the above-known parameters, the parameters to be identified of the simulation model are set as $K_s = 1 \times 10^6$ Nm·rad^{-1}, $B_m = 0.005$ Nm·rad^{-1}·s, $B_L = 20$ Nm·rad^{-1}·s, T_{cm}^{+} =0.1 Nm, $T_{cm}^{-} = -0.1$ Nm, $T_{cL}^{+} = 5$ Nm, $T_{cL}^{-} = -5$ Nm, $2\Delta = 1$ arcmin, and $n_1 = 3$. Reference will be made to the velocity control loop, and the loop is closed on the load side, the speed measurements being actually numerical differentiations of position measurements obtained with an encoder. A PI (Proportional Integral) regulator is used, whose tuning had already been performed independently of this article. This tuning, however, is inessential here, as the goal is just the validation of the model and identification method. The sine signal with an amplitude of 30°/s and frequency of 1 Hz is input as the command, and the identification results without load and with load are shown in Figure 5a,b, respectively. In addition, Table 1 lists the converged values.

It can be seen from Figure 5 and Table 1 that the multi-parameter online identification method proposed in this paper can accurately estimate the values of J_L, B_m, B_L, K_s, T_{cm}^{+}, T_{cm}^{-}, T_{cL}^{+}, T_{cL}^{-}, and Δ with and without load, and the steady-state error is not more than 10%.

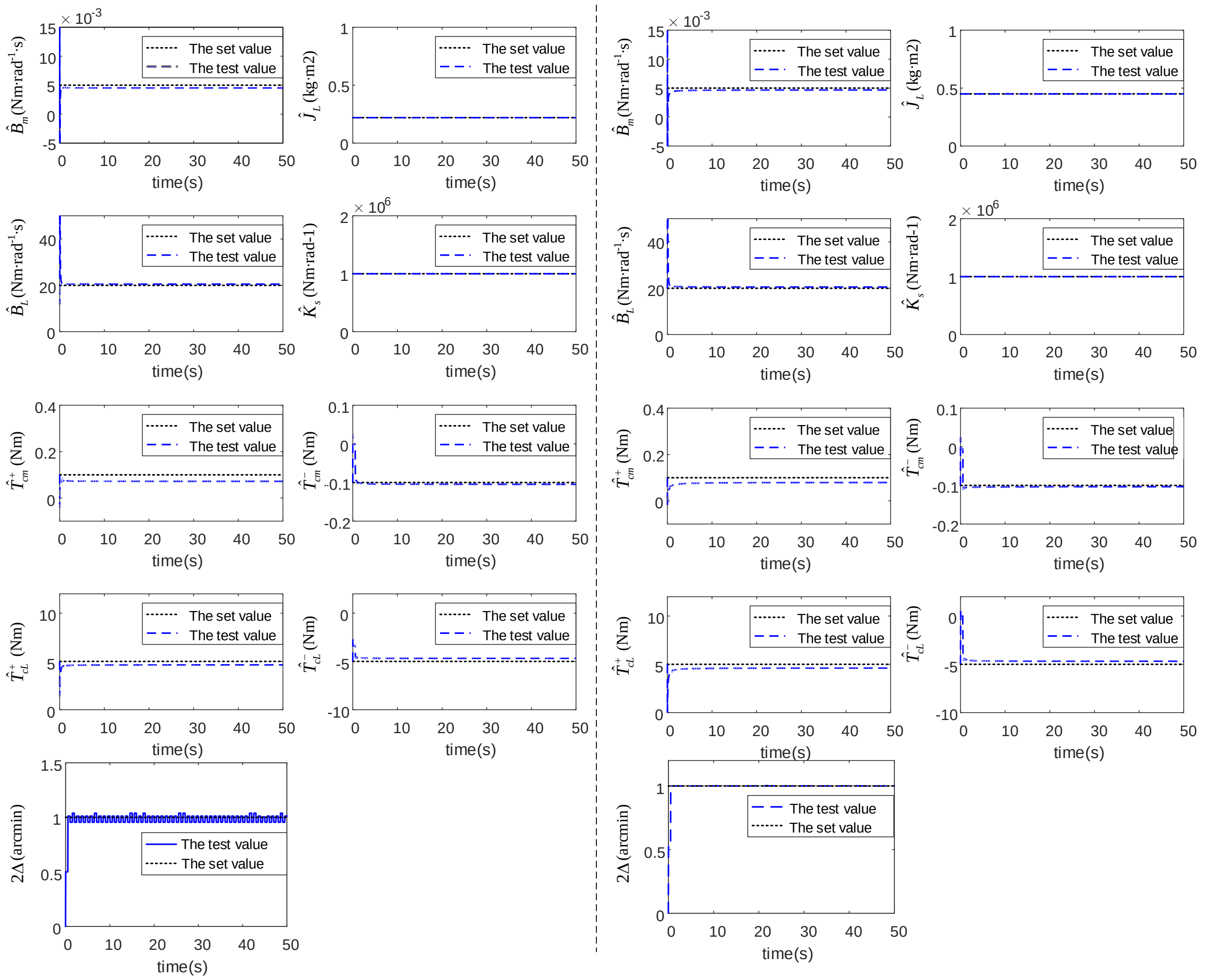

(a) **(b)**

Figure 5. Convergence process of the multi-parameter online identification in the simulation. (**a**) Without load; (**b**) With load.

Table 1. The converged values of the identification results in the simulation.

	Without Load			**With Load**		
Parameters	**The Set Value**	**The Estimated Value**	**Error (%)**	**The Set Value**	**The Estimated Value**	**Error (%)**
$\hat{B}_m$ (Nm·rad^{-1}·s)	0.005	0.0045	10	0.005	0.00467	6.6
$\hat{J}_L$ (kg·m^2)	0.22	0.22	0	0.45	0.406	9.78
$\hat{B}_L$ (Nm·rad^{-1}·s)	20	20.51	2.55	20	20.54	2.7
$\hat{K}_s$ (Nm·rad^{-1})	1×10^6	1×10^6	0	1×10^6	1×10^6	0
$\hat{T}^+_{cm}$ (Nm)	0.1	0.092	8	0.1	0.0904	9.6
$\hat{T}^-_{cm}$ (Nm)	−0.1	−0.1046	0.46	−0.1	−0.1034	0.34
$\hat{T}^+_{cL}$ (Nm)	5	4.643	7.14	5	4.612	7.76
$\hat{T}^-_{cL}$ (Nm)	−5	−4.683	6.34	−5	−4.68	6.4
2Δ (arcmin)	1	0.9~1.1	10	1	1~1.1	10

4.2. Experimental Results

A series of experiments were carried out to validate the effectiveness of the multi-parameter online identification method. The experimental projects are mainly divided into two parts: The multi-parameter online identification tests were carried out in part one. The second part validated the accuracy of the dynamic model by updating the model parameters in real-time based on the online identification results.

4.2.1. Multi-Parameter Online Identification Results

The multi-parameter online identification results of the actual system before and after adding the mass blocks are shown in Figure 6a,b, respectively, and whose converged values are listed in Table 2.

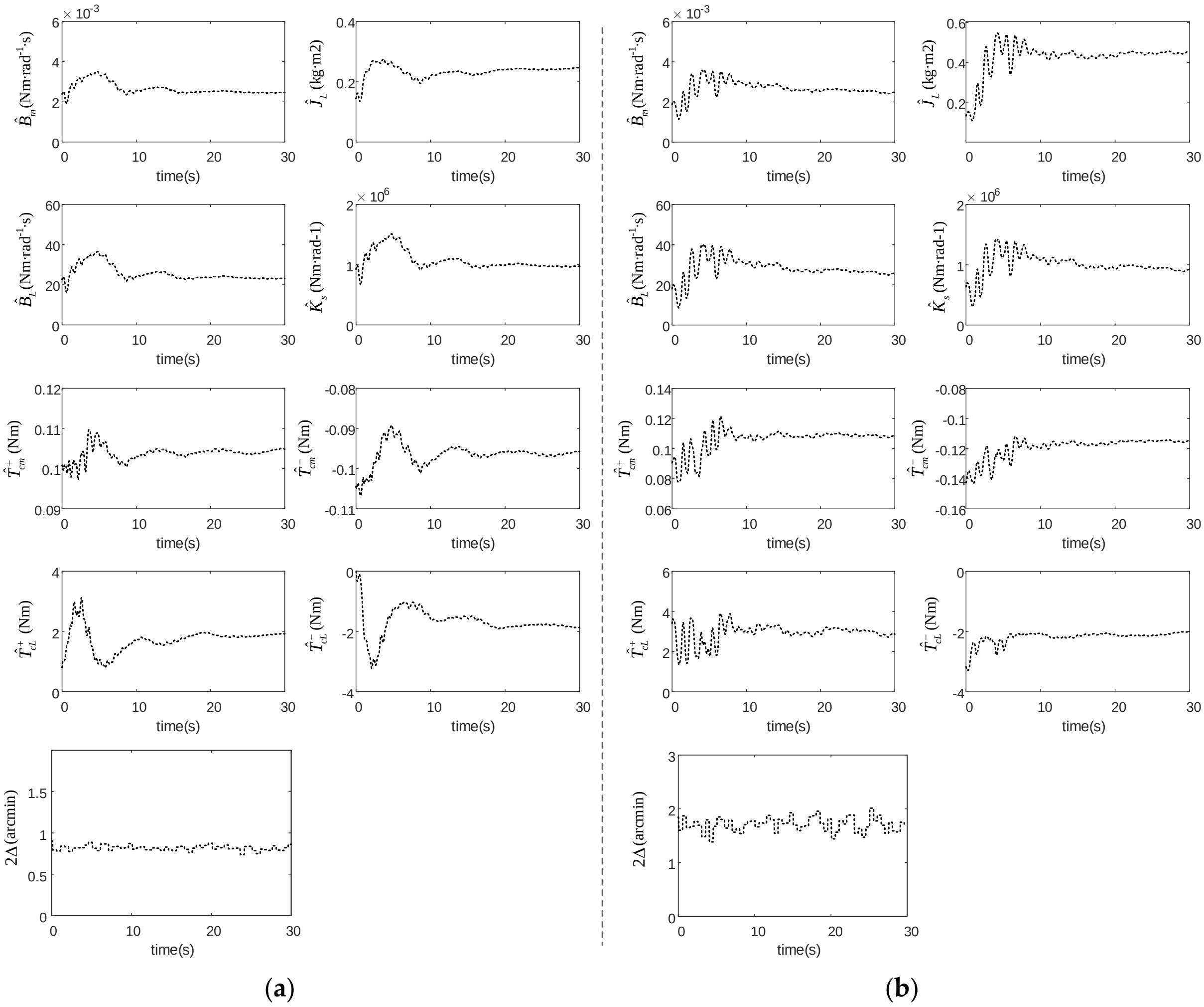

Figure 6. Convergence process of multi-parameter online identification in the experiment. (**a**) Without load; (**b**) With load.

The identification results show that the multi-parameter online identification method can not only recognize the adjustment of load but also detect the change of backlash and friction when the load varies. The backlash and friction torque increase with the increase of the mass blocks. The reason is that with the mass blocks added, the pressure on the bearing increased, and the Coulomb friction torque is proportional to the pressure, so the friction torque increased. When the increment of friction torque is greater than the inertia torque, the angular forward movement of the load due to the inertia would reduce, so the measured backlash would enlarge.

Table 2. The converged values of the identification results in the experiment.

Parameters	Without Load	With Load
$\hat{B}_m$ (Nm·rad^{-1}·s)	2.4×10^{-3}	2.4×10^{-3}
$\hat{J}_L$ (kg·m^2)	0.246	0.453
$\hat{B}_L$ (Nm·rad^{-1}·s)	23.17	25.23
$\hat{K}_s$ (Nm·rad^{-1})	9.7×10^5	8.9×10^5
$\hat{T}_{cm}^{+}$ (Nm)	0.1	0.11
$\hat{T}_{cm}^{-}$ (Nm)	−0.095	−0.12
$\hat{T}_{cL}^{+}$(Nm)	1.9	2.89
$\hat{T}_{cL}^{-}$ (Nm)	−1.86	−2.01
2Δ (arcmin)	0.82	1.74

4.2.2. Dynamic Model Validation Results

By live updating all parameters identified online to the model, we compared the similarity between the model and the actual system. Figure 7a,b show the comparison results under no load and load, respectively.

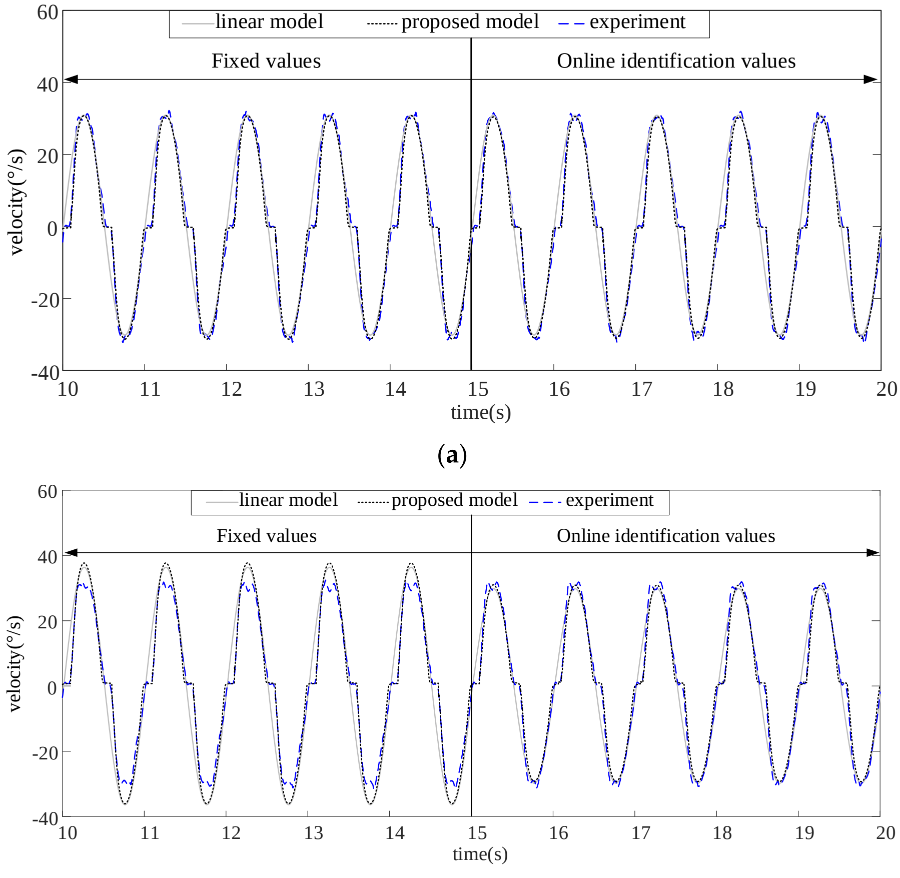

(**a**)

(**b**)

Figure 7. Dynamic model experimental verification. (**a**) Without load; (**b**) With load.

In the figure, the solid gray curve is the linear dual-inertia model without backlash and nonlinear friction torque, the black dotted curve represents the model proposed in this paper, and the blue dashed curve is the velocity of the actual system collected by the absolute encoder. When time < 15 s, the value of the parameters is set to the initial value and fixed. When time > 15 s, the parameters are live updated through online estimation.

It can be seen from Figure 7a that the traditional linear model has a low fitting degree with the actual system. However, the proposed model is highly similar to the actual system, indicating that the initial value assigned to the proposed model is consistent with the system. When there is load, Figure 7b shows that the velocity of the fixed value model is higher than that of the actual velocity (time < 15 s). After switching to the values identified online (time > 15 s), the model is highly consistent with the actual system again. The reason is that after adding the mass blocks, the moment of inertia of the load increase, while the values of the fixed value model are still the initial value, which is less than the actual system, resulting in the model velocity being greater than the actual system. The experimental results show that although the system characteristics have changed after adjusting the load, the model can still well monitor the system throughmulti-parameter online identification.

The fitting degrees between the two models and the actual system are expressed by the root mean square of error (RMSE), and the results are shown in Table 3. It can be seen from Table 3 that, compared with the fixed values linear model, the RMSE of the proposed model with load can be reduced from 6.83 to 2.37, which is improved by 65.3% at most.

Table 3. The RMSE of the model and actual system.

Experiments	Without Load	With Load
Linear model (fixed values)	5.23	6.83
Linear model (online identification values)	5.16	4.36
Proposed model(fixed values)	2.12	3.52
Proposed model (online identification values)	2.11	2.37

5. Conclusions

An adaptive multi-parameter estimation method is proposed to monitor the state of the ISP with high accuracy when the load is changed. The dual-inertia dynamic model considering the backlash and the nonlinear friction torque of the motor and load is formed, and the online identification expressions of the parameters of the motor and load are obtained by using forward Euler method. Then, an adaptive multi-parameter estimation method based on the RELS is put forward. Finally, the effectiveness of the multi-parameter estimation method is verified by simulations and experiments, and the following two conclusions are obtained:

(1) Simulation and experimental results show that when the load changes, the multi-parameter estimation method can simultaneously identify the changes of J_L, B_m, B_L, K_s, T_{cm}^{+}, T_{cm}^{-}, T_{cL}^{+}, T_{cL}^{-}, and Δ at one time, and the steady-state error is less than 10%, which is more comprehensive than previous studies;

(2) Compared with the traditional linear dual-inertia model neglecting the backlash and nonlinear friction torque, the RMSE between the proposed model and the actual system can be reduced from 6.83 to 2.37, which is improved by 65.3% at most.

Thus, the proposed model and adaptive multi-parameter estimation method can realize the status monitoring of the ISP when the loads are frequently changed and provide a basis for the adaptive high-precision control.

Author Contributions: Conceptualization, J.Z.; methodology, J.Z.; software, B.L. and N.C.; validation, Z.W. and N.C.; formal analysis, J.Z.; investigation, J.Z.; resources, J.Z.; data curation, J.Z.; writing—original draft preparation, J.Z.; writing—review and editing, X.X. and D.F.; visualization, J.Z.; supervision, X.X. and D.F.; project administration, D.F.; funding acquisition, D.F. All authors have read and agreed to the published version of the manuscript.

Funding: This research was funded by the National Key R and D Program of China (Grant No. 2019YFB2004704).

Institutional Review Board Statement: Not applicable.

Informed Consent Statement: Not applicable.

Data Availability Statement: Not applicable.

Conflicts of Interest: The authors declare no conflict of interest.

References

1. Jiang, X.; Fan, D.; Fan, S.; Xie, X.; Chen, N. High-precision gyro-stabilized control of a gear-driven platform with a floating gear tension device. *Front. Mech. Eng.* **2021**, *16*, 487–503. [CrossRef]
2. Weng, J.; Liu, J.; Jiao, M.; Kou, K. Analysis and on-line compensation of gravity disturbance in a high-precision inertial navigation system. *GPS Solut.* **2020**, *24*, 83. [CrossRef]
3. Ren, W.; Luo, Y.; He, Q.; Zhou, X.; Deng, C.; Mao, Y.; Ren, G. Stabilization Control of Electro-Optical Tracking System with Fiber-Optic Gyroscope Based on Modified Smith Predictor Control Scheme. *IEEE Sens. J.* **2018**, *18*, 8172–8178. [CrossRef]
4. Yang, Y.; Lin, Z.; Liu, F. Stable Imaging and Accuracy Issues of Low-Altitude Unmanned Aerial Vehicle Photogrammetry Systems. *Remote Sens.* **2016**, *8*, 316. [CrossRef]
5. Zhou, X.; Shi, Y.; Li, L.; Yu, R.; Zhao, L. A High Precision Compound Control Scheme Based on Non-singular Terminal Sliding Mode and Extended State Observer for an Aerial Inertially Stabilized Platform. *Int. J. Control Autom. Syst.* **2020**, *18*, 1498–1509. [CrossRef]
6. Yan, L.; Dai, J.; Zhao, Y.; Chen, C. Real-Time 3D Mapping in Complex Environments Using a Spinning Actuated LiDAR System. *Remote Sens.* **2023**, *15*, 963. [CrossRef]
7. Wang, S.; Zhu, R. Nonlinear dynamic analysis of GTF gearbox under friction excitation with vibration characteristics recognition and control in frequency domain. *Mech. Syst. Signal Process.* **2021**, *151*, 107373. [CrossRef]
8. Cao, Z.; Chen, Z.; Jiang, H. Nonlinear dynamics of a spur gear pair with force-dependent mesh stiffness. *Nonlinear Dyn.* **2020**, *99*, 1227–1241. [CrossRef]
9. Siyu, C.; Jinyuan, T.; Caiwang, L.; Qibo, W. Nonlinear dynamic characteristics of geared rotor bearing systems with dynamic backlash and friction. *Mech. Mach. Theory* **2011**, *46*, 466–478. [CrossRef]
10. Harandi, M.R.J.; Khalilpour, S.A.; Taghirad, H.D.; Romero, J.G. Adaptive control of parallel robots with uncertain kinematics and dynamics. *Mech. Syst. Signal Process.* **2021**, *157*, 107693. [CrossRef]
11. Li, S.; Liu, Z. Adaptive Speed Control for Permanent-Magnet Synchronous Motor System with Variations of Load Inertia. *IEEE Trans. Ind. Electron.* **2009**, *56*, 3050–3059. [CrossRef]
12. Ding, J.; Zhang, W. Finite-time adaptive control for nonlinear systems with uncertain parameters based on the command filters. *Int. J. Adapt. Control Signal Process.* **2021**, *35*, 1754–1767. [CrossRef]
13. Wang, S.; Na, J. Parameter Estimation and Adaptive Control for Servo Mechanisms with Friction Compensation. *IEEE Trans. Ind. Inform.* **2020**, *16*, 6816–6825. [CrossRef]
14. Zhou, J.; Wen, C.; Wang, W. Adaptive control of uncertain nonlinear systems with quantized input signal. *Automatica* **2018**, *95*, 152–162. [CrossRef]
15. She, J.; Wu, L.; Zhang, C.-K.; Liu, Z.-T.; Xiong, Y. Identification of Moment of Inertia for PMSM Using Improved Modelreference Adaptive System. *Int. J. Control Autom. Syst.* **2022**, *20*, 13–23. [CrossRef]
16. Liu, F.; Kang, E.; Cui, N. Single-loop model prediction control of PMSM with moment of inertia identification. *IEEJ Trans. Elec. Electron. Eng.* **2020**, *15*, 577–583. [CrossRef]
17. Kim, S. Moment of Inertia and Friction Torque Coefficient Identification in a Servo Drive System. *IEEE Trans. Ind. Electron.* **2019**, *66*, 60–70. [CrossRef]
18. Lian, C.; Xiao, F.; Gao, S.; Liu, J. Load Torque and Moment of Inertia Identification for Permanent Magnet Synchronous Motor Drives Based on Sliding Mode Observer. *IEEE Trans. Power Electron.* **2019**, *34*, 5675–5683. [CrossRef]
19. Yang, M.; Liu, Z.; Long, J.; Qu, W.; Xu, D. An Algorithm for Online Inertia Identification and Load Torque Observation via Adaptive Kalman Observer-Recursive Least Squares. *Energies* **2018**, *11*, 778. [CrossRef]
20. Nevaranta, N.; Derammelaere, S.; Parkkinen, J.; Vervisch, B.; Lindh, T.; Stockman, K.; Niemela, M.; Pyrhonen, O.; Pyrhonen, J. Online Identification of a Mechanical System in Frequency Domain Using Sliding DFT. *IEEE Trans. Ind. Electron.* **2016**, *63*, 5712–5723. [CrossRef]
21. Amini, F.; Aghabarari, E. Online parameter estimation and adaptive control with limited information in structures. *J. Vib. Control* **2022**, *28*, 2717–2731. [CrossRef]
22. Alvaro-Mendoza, E.; De León-Morales, J.; Salas-Peña, O. State and parameter estimation for a class of Nonlinear Systems based on Sliding Mode Approach. *ISA Trans.* **2021**, *112*, 99–107. [CrossRef] [PubMed]
23. Xu, Z.; Du, L.; Wang, H.; Deng, Z. Particle swarm optimization-based algorithm of a symplectic method for robotic dynamics and control. *Appl. Math. Mech.-Engl. Ed.* **2019**, *40*, 111–126. [CrossRef]
24. Wang, X.; Liu, B.; Mei, X.; Yun, X.; Li, X.; Li, Q.; Wang, X. Genetic algorithm for dynamic parameters estimation of the machine tool worktable using the residual vibration signal. *J. Vib. Control* **2022**, *28*, 1433–1440. [CrossRef]
25. Zhang, Q.; Fan, Y. The Online Parameter Identification Method of Permanent Magnet Synchronous Machine under Low-Speed Region Considering the Inverter Nonlinearity. *Energies* **2022**, *15*, 4314. [CrossRef]
26. Erkorkmaz, K.; Altintas, Y. High speed CNC system design. Part III: High speed tracking and contouring control of feed drives. *Int. J. Mach. Tools Manuf.* **2001**, *41*, 1637–1658. [CrossRef]